Materials and Design 60 (2014) 368–379

Contents lists available at ScienceDirect

Materials and Design

journal homepage: www.elsevier.com/locate/matdes

# Influence of the plastic anisotropy modelling in the reverse deep drawing process simulation

D.M. Neto [a,*], M.C. Oliveira [a], J.L. Alves [b], L.F. Menezes [a]

[a] CEMUC, Department of Mechanical Engineering, University of Coimbra, Polo II, Rua Luís Reis Santos, Pinhal de Marrocos, 3030-788 Coimbra, Portugal
[b] CT2M, Department of Mechanical Engineering, University of Minho, Campus de Azurém, 4800-058 Guimarães, Portugal

ARTICLE INFO

*Article history:*
Received 15 January 2014
Accepted 2 April 2014
Available online 13 April 2014

*Keywords:*
Reverse deep drawing
Finite element simulation
Planar anisotropy
Yield criteria
Strain paths

ABSTRACT

This study deals with the description of the anisotropic behaviour of the mild steel sheet used in the reverse deep drawing process of a cylindrical cup, which was proposed as benchmark at the Numisheet'99 conference. The effect of the yield criterion on the numerical results is analysed using three yield functions, von Mises, Hill'48 and Barlat Yld'91, combined with the Swift hardening law. The anisotropy parameters of the Hill'48 model are identified using either the yield stresses or *r*-values, obtained from the uniaxial tensile test at three different directions. On the other hand, the anisotropy parameters of the Yld'91 are determined taking into account both the yield stresses and *r*-values, minimizing an objective function. The comparison between experimental and numerical results is presented, being the punch force evolution and the thickness distribution along the cup wall the principal variables under study. In both forming stages, the predicted punch force evolution is close to the experimental one, whatever the yield criterion adopted. Nevertheless, the cup wall thickness distribution is strongly influenced by the yield criteria, being clearly overestimated by the von Mises yield criterion. On the other hand, the Yld'91 yield criterion provides a thickness distribution closer to the experimental one, for both forming stages. The strain paths during both forming stages ranges from uniaxial compression, when the material flows between the die and blank-holder, to plane strain in the cup wall, whereas the important strain path changes occurs in the die radius.



## 1. Introduction

The numerical analysis of sheet metal forming processes is nowadays an indispensable tool in the virtual product conception, particularly in the automotive and aerospace industries. The strong reduction of development periods in the car manufacturing industry, imposed in the last decades by the highly competitive global world market, leads to the redefinition of the conventional manufacturing procedures [1]. Consequently, the traditional tool design methods based on a trial-and-error or empirical procedure are gradually replaced by the usage of finite element simulation systems [2–4]. Gantar et al. [5] conclude that the numerical simulation can be successfully used to optimize the variable input process parameters in order to solve some technological problems, such as fracture, necking, wrinkling and springback. However, accurate simulation results are mandatory to correctly predict the entire forming operations.

The mechanical modelling of sheet metal forming leads to a strongly nonlinear problem due to the nonlinearity induced by the frictional contact, the geometrical nonlinearity produced by large deformation and the material nonlinearity due to the elastoplastic behaviour [6]. Concerning the last nonlinearity, the constitutive material model should comprises both the work hardening law and the yield criterion to account the anisotropy of mechanical properties, which results from the rolling process used in the production of sheet metals. Yoon et al. [7] point out that the material anisotropy should be taken into account for accurately sheet forming analysis of cylindrical cups, since it dictates the strain distribution and consequently the sheet metals formability. Several yield functions have been proposed to describe the anisotropic plastic flow of sheet metal. The current study focus on three-dimensional yield criteria since the metallic sheet will be modelled using solid finite elements. The quadratic anisotropic yield criterion proposed by Hill [8] is the generalization of the von Mises criterion [9] for anisotropic materials. The main drawback of this yield function is its limitation to correctly

* Corresponding author. Tel.: +351 239790700; fax: +351 239790701.
*E-mail addresses:* diogo.neto@dem.uc.pt (D.M. Neto), marta.oliveira@dem.uc.pt (M.C. Oliveira), jlalves@dem.uminho.pt (J.L. Alves), luis.menezes@dem.uc.pt (L.F. Menezes).

http://dx.doi.org/10.1016/j.matdes.2014.04.008
0261-3069/

**Nomenclature**

| | |
|---|---|
| $Y$ | flow stress (MPa) |
| $K$, $\varepsilon_0$ and $n$ | parameters of the Swift law |
| $F$, $G$, $H$ ... | parameters of the Hill 1948 yield criterion |
| $\bar{\sigma}$ | equivalent tensile stress (MPa) |
| $c_1$, $c_2$, $c_3$... | parameters of the Barlat 1991 yield criterion |
| $m$ | parameter defining the shape of the yield surface in Barlat 1991 |
| $\theta$ | direction with rolling direction (°) |
| $r_\theta$ | coefficient of plastic anisotropy for a direction $\theta$ with the rolling direction |
| $\sigma_\theta$ | uniaxial yield stress at a direction $\theta$ with the rolling direction (MPa) |

describe the behaviour of various face-centred cubic (FCC) metals, namely some aluminium alloys [10]. However, in case of body-centred cubic (BCC) metals it is the most widely used [11]. In order to overcome the previous mentioned limitation, various non-quadratic yield criteria were developed. Barlat et al. [12] proposed a non-quadratic anisotropic yield criterion based in the stress field with six-component yield function, being particularly adequate for aluminium alloys. Cazacu and Barlat [13] introduced generalized invariants of the stress deviator which allows transform any isotropic yield criterion to anisotropy for various type of material symmetry. However, it should be pointed out that there is no mathematical proof of convexity for this yield function. Besides, the identification of the material parameters requires different experimental tests due to the high number of anisotropic parameters involved, being the simple uniaxial tensile tests insufficient.

In the present study, numerical simulations using the finite element method are performed to evaluate the influence of both the yield criteria and the approach adopted to identify its parameters. The selected example is the reverse deep drawing process of a cylindrical cup, proposed as benchmark at the Numisheet'99 conference [14]. This study complements the work carried out by Thuillier et al. [15], which investigated the influence of the work hardening law on the numerical results, adopting the same sheet forming example. The material selected in both studies is the mild steel DDQ. Three yields functions are considered, the von Mises [9], Hill'48 [8] and the Barlat Yld'91 [12], being the anisotropic parameters of the Hill'48 criterion identified based on either the $r$-value or the yield stress obtained from uniaxial tensile tests. The comparison between the numerical and experimental results is presented to evaluate the effectiveness of the yield criterion selected, as well as the parameter identification strategy adopted. The main process parameters studied in each stage are the punch force evolution, the thickness distribution along the cup wall and the earing profile. Moreover, the predicted cup wall thickness distribution is directly correlated with the strain paths that occurred during both forming stages.

## 2. Reverse deep drawing process

The deep drawing process is one of the more extensively used sheet metal forming process. In this process, the forming parts are usually obtained in a single-stage, but in some conditions multi-stage operation is required due to geometrical complexity or formability problems [16]. Nevertheless, the minimum number of forming stages necessary to obtain the desired part without failure depends on many process parameters, being its determination, as well the shape of the tools for each stage, an enormous challenge [17]. Since the maximum drawing ratio $R_0/R_i$ ($R_0$ and $R_i$ are the blank and punch radius, respectively) obtained with a single-stage operation is usually about two [18], the redrawing process is typically adopted when large drawing ratios are necessary.

Generally the redrawing process is classified in two categories: direct and reverse. The first drawing operation is the same in both process types, whereas the difference occurs at the redrawing stage, as shown schematically in Fig. 1. In the direct redrawing process (Fig. 1(a)) the punch in each stage is always in contact with the same blank side, while in the reverse redrawing (Fig. 1(b)) the punch motion during the second stage arises in the opposite direction. Since the number of bending–unbending operations is smaller in the reverse than in the direct redrawing (compare the material flow as shown in Fig. 1), the required punch force is lower in the reverse redrawing [18]. Moreover, the surface aspect is better in the reverse process since the outside of the part is in contact only once with the die radius [19].

The first analytical analysis of the multi-stage drawing processes was developed by Chung [20] under large simplifications on the radial strain. Zharkov [21] considers sheet thickness changes in its analytical model and takes into account strain hardening. Although the numerical simulation of single-stage deep drawing operations has been investigated by several researchers, the multi-stage drawing process comprises additional complex deformation mechanisms, becoming its numerical simulation more difficult. Teodosiu et al. [22] studied the drawing and redrawing operations using two-dimensional axisymmetric finite element analysis, which is limited to normal anisotropy for the sheet. On the other hand, Kim et al. [23] perform three dimensional finite element analysis of multi-stage deep drawing in order to define the tool design in each intermediate stage using the thickness strain distribution as objective function, taking into account planar anisotropy. The optimization of the direct redrawing process of molybdenum sheets including ironing was performed by Kim and Hong [24], using a two-dimensional axisymmetric finite element analysis based on isotropic material behaviour. Parsa et al. [25] studied the behaviour of two-layer (aluminium–stainless-steel) laminated sheets during two-stage deep drawing, comparing experiment and numerical results. They found that the maximum drawing ratio is reached in direct redrawing when the punch is in contact with the stainless-steel, while applying reverse redrawing the aluminium should be in contact with the punch to attain the maximum drawing ratio.

## 3. Finite element simulation

The example selected in the present study is the reverse deep drawing process of a cylindrical cup, proposed as benchmark at the Numisheet'99 conference [14], which is schematically presented in Fig. 2. The numerical simulations were performed with the DD3IMP in-house finite element code, which has been specifically developed to simulate sheet metal forming processes [6]. Its key feature is the use of a fully implicit algorithm of Newton–Raphson type to solve, within a single iterative loop, the nonlinearities related with both the mechanical behaviour and the frictional contact. The kinematic description of the deformation process is described by an updated Lagrangian scheme. The frictional contact is defined by the Coulomb's classical law and treated with a mixed

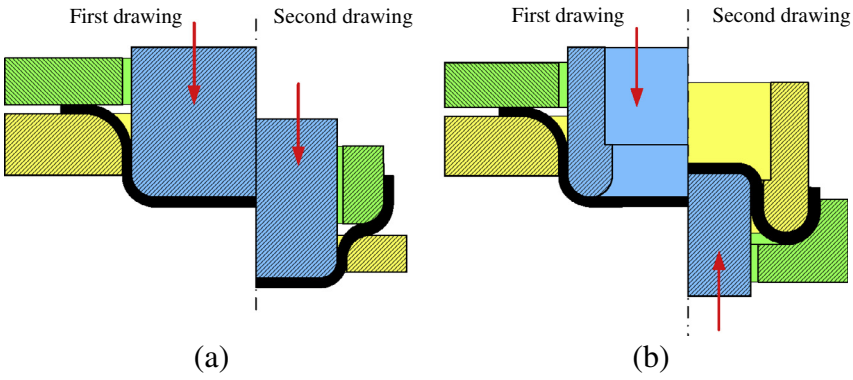


**Fig. 1.** Scheme of the two-stage deep drawing process: (a) direct redrawing; and (b) reverse redrawing.

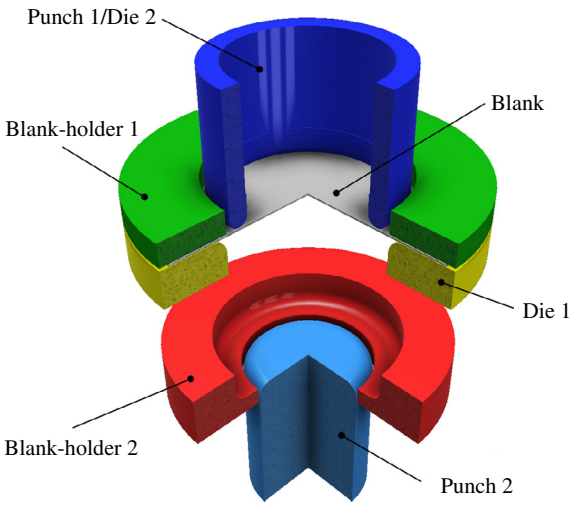


**Fig. 2.** Scheme of the forming tools used in the reverse deep drawing of a cylindrical cup.

formulation, using the augmented Lagrangian approach proposed by Alart and Curnier [26]. The contact occurs between a deformable sheet and rigid tools modelled with Nagata patches [27]. The sheet is discretized with solid elements, allowing an accurate evaluation of the contact forces and the stress gradients through the thickness. On the other hand, since static implicit codes check the equilibrium conditions in each time step, the use of solid elements leads is more CPU time-consuming. Therefore, some high performance computing techniques have been incorporated, such as introducing OpenMP directives in the most time consuming branches of the code [28].

### 3.1. Constitutive model

The material considered in this study is the mild steel DDQ with a blank thickness of 0.98 mm. The elastoplastic constitutive model adopted considers anisotropic plastic behaviour, being defined by: (i) an associated flow rule; (ii) a yield criterion and (iii) a hardening law. Yoon et al. [7] pointed out that the material behaviour based on an anisotropic yield function and simply isotropic hardening is acceptable to accomplish accurate results in the numerical simulation of cylindrical cups forming. Thus, only isotropic hardening is considered in this study, in opposition to the analysis performed by Thuillier et al. [15]. This assumption is known to be questionable, but this model is still widely used. Besides, the available data from the benchmark committee does not include the required experimental tests (e.g. Bauschinger shear tests) to perform the parameters identification of the kinematic hardening model. The isotropic work hardening behaviour is modelled by the Swift law, which is most suitable for mild steels, being expressed by:

$$Y = K(\varepsilon_0 + \bar{\varepsilon}^p)^n \quad \text{with} \quad \varepsilon_0 = \left(\frac{\sigma_0}{K}\right)^{1/n}, \tag{1}$$

where $Y$ is the flow stress and $\bar{\varepsilon}^p$ is the equivalent plastic strain. The material parameters $K$, $n$ and $\sigma_0$ are evaluated using only the uniaxial tensile test results provided by the benchmark committee. The material mechanical behaviour follows Hooke's law in the elastic regime, being described by the Young modulus and the Poisson ratio.

The yield criterion expresses the relationship between the stress components in the transition from the elastic to the plastic regime, which evolution is dictated by Eq. (1). Three yield functions are adopted in this study: (i) von Mises isotropic, (ii) Hill'48 anisotropic and (iii) Yld'91 non-quadratic anisotropic model. The most commonly used yield criteria for isotropic materials are Tresca [29] and von Mises [9]. However, the metallic sheets exhibits an anisotropic behaviour characteristic of the rolling process. Hence, Hill [8] proposed an anisotropic yield criterion, considering that the material has an anisotropic behaviour along three orthogonal symmetry planes (orthotropic behaviour). The yield criterion is expressed by the quadratic function:

$$F(\sigma_{yy} - \sigma_{zz})^2 + G(\sigma_{zz} - \sigma_{xx})^2 + H(\sigma_{xx} - \sigma_{yy})^2 + 2L\tau_{yz}^2 + 2M\tau_{zx}^2 + 2N\tau_{xy}^2 = \bar{\sigma}^2, \tag{2}$$

where $\sigma_{xx}$, $\sigma_{yy}$, $\sigma_{zz}$, $\tau_{yz}$, $\tau_{zx}$ and $\tau_{xy}$ are the components of the Cauchy stress tensor defined in the orthotropic frame, while $F$, $G$, $H$, $L$, $M$ and $N$ are the Hill'48 parameters that define the anisotropic behaviour, and $\bar{\sigma}$ is the equivalent tensile stress. In the case of sheet metals, the orthotropic frame axis $x$ is usually parallel to the rolling direction, $y$ is parallel to the transverse direction and $z$ is collinear with the normal direction.

The Yld'91 yield criterion proposed by Barlat et al. [12] is an extension to orthotropy of the Hosford [30] isotropic yield criterion. It can be expressed by the following non-quadratic function:

$$|S_1 - S_2|^m + |S_2 - S_3|^m + |S_3 - S_1|^m = 2\bar{\sigma}^m, \tag{3}$$

where $S_1$, $S_2$ and $S_3$ are the principal values of the isotropic plastic equivalent deviatoric stress tensor $\mathbf{S} = \mathbf{L}:\boldsymbol{\sigma}$, which is obtained from the linear transformation $\mathbf{L}$ applied to the Cauchy stress tensor $\boldsymbol{\sigma}$. The exponent $m$ characterizes the shape of the yield surface, which depends on the material crystallographic structure, being 6 for BCC and 8 for FCC materials [31]. The Yld'91 anisotropy parameters are indirectly defined through the linear transformation on the stress deviator, given by:

$$\mathbf{L} = \frac{1}{3}\begin{bmatrix} (c_2+c_3) & -c_3 & -c_2 & 0 & 0 & 0 \\ -c_3 & (c_3+c_1) & -c_1 & 0 & 0 & 0 \\ -c_2 & -c_1 & (c_1+c_2) & 0 & 0 & 0 \\ 0 & 0 & 0 & 3c_4 & 0 & 0 \\ 0 & 0 & 0 & 0 & 3c_5 & 0 \\ 0 & 0 & 0 & 0 & 0 & 3c_6 \end{bmatrix}, \quad (4)$$

where $c_1$, $c_2$, $c_3$, $c_4$, $c_5$ and $c_6$ are the anisotropy parameters.

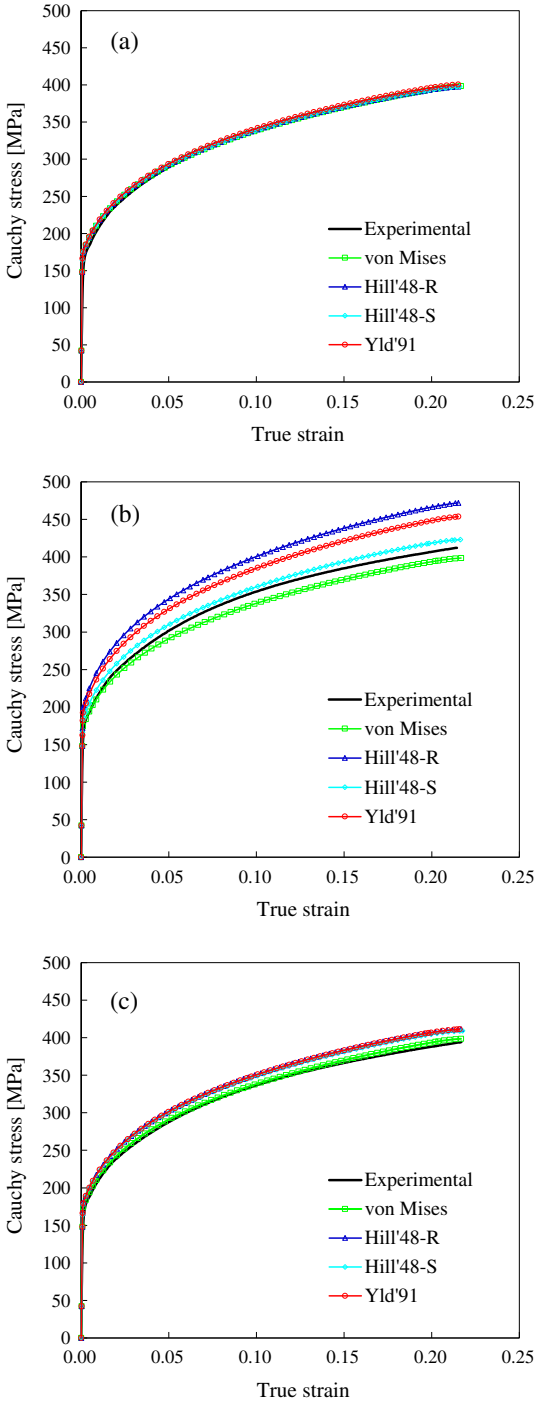


**Fig. 3.** Experimental and numerical uniaxial tensile tests obtained at: (a) 0° with the RD; (b) 45° with the RD; and (c) 90° with the RD.

### 3.2. Material parameters identification

The material parameters for the work hardening law were identified with the conventional uniaxial tensile tests provided by the benchmark committee [14]. Although experimental data from other tests have been used for more advanced constitutive models (e.g. [11]), in the present work the available experimental data is limited to standard tensile tests. Hence, in order to estimate the anisotropy of DDQ mild steel, the specimens were obtained at 0°, 45° and 90° with the rolling direction (RD). Fig. 3 presents the experimental stress–strain curves measured from uniaxial tension tests obtained in the three different directions with the RD. The isotropic hardening behaviour defined by the Swift law was identified directly by fitting the stress–strain curve obtained along the RD (Fig. 3(a)). The identified material parameters for the Swift hardening law are given in Table 1, as well the elastic properties of the mild steel defined by the Young modulus and the Poisson ratio. In order to fit accurately the stress–strain curve also for high strain values, the initial yield stress predicted by the Swift law (172 MPa) in the RD is slightly lower than the experimental value, given in Table 2.

The uniaxial tensile tests are also used to evaluate material parameters of the yield criterion. The coefficient of plastic anisotropy associated to the direction $\theta$ with the RD is defined by:

$$r_\theta = \frac{\varepsilon^p_{22}}{\varepsilon^p_{33}} = \frac{\varepsilon^p_{22}}{-\left(\varepsilon^p_{11}+\varepsilon^p_{22}\right)}, \quad (5)$$

where $\varepsilon^p_{11}$ and $\varepsilon^p_{22}$ are the true plastic strains in the axial and transverse directions of the specimen, respectively. The uniaxial $r$-values are evaluated during the tensile test using extensometers in both directions. Fig. 4 presents the experimental anisotropy coefficient determined at three directions with the rolling direction, which is defined by the slope of the straight line fitting the experimental points. Thus, the experimental $r$-values obtained from the linear fitting in Fig. 4 are presented in Table 2 together with the yield stresses measured in the same directions, which are the basic mechanical properties provided by the benchmark committee.

In the present study, the identification of the anisotropy parameters for the Hill'48 model is carried out using two different approaches. The classical approach uses the $r$-values from three uniaxial tensile tests (0°, 45° and 90° with the RD), being labelled by 'Hill'48-R'. On the other hand, the second approach resorts to the set of three yield stresses from uniaxial tension tests, which is labelled by 'Hill'48-S'. Since it is very difficult to evaluate the through thickness anisotropic behaviour in metallic sheets, the parameters defining those properties are assumed isotropic, i.e. for both approaches of the Hill'48 criterion $L = M = 1.5$. For the Hill'48 yield criterion under plane stress conditions ($\sigma_{zz} = \tau_{yz} = \tau_{zx} = 0.0$), the uniaxial yield stress at a direction $\theta$ with the rolling direction is given by:

**Table 1**
Elastic properties and Swift hardening law parameters of DDQ mild steel.

| Elastic properties | | Swift law | | |
|---|---|---|---|---|
| Young's modulus (GPa) | Poisson's ratio | $K$ (MPa) | $\sigma_0$ (MPa) | $n$ |
| 210 | 0.30 | 568.34 | 172.0 | 0.233 |

**Table 2**
Mechanical properties of DDQ mild steel provided by the benchmark committee [14].

| Angle with RD (°) | Yield stress (MPa) | Max uniform strain | $r$-value |
|---|---|---|---|
| 0 | 176 | 0.24 | 1.73 |
| 45 | 185 | 0.22 | 1.23 |
| 90 | 180 | 0.23 | 2.02 |

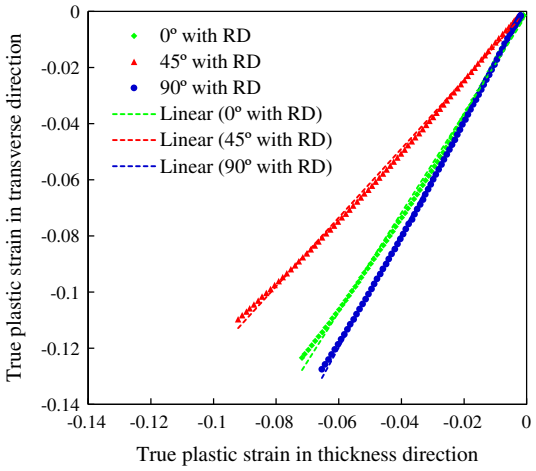


**Fig. 4.** Experimental evaluation of the anisotropy coefficient for three directions with the rolling direction.

$$\sigma_\theta = \frac{\bar{\sigma}}{\sqrt{F\sin^4\theta + G\cos^4\theta + H\cos^2 2\theta + 2N\sin^2\theta\cos^2\theta}}, \tag{6}$$

while the uniaxial anisotropy at the same direction $\theta$ predicted by the yield criterion is defined by:

$$r_\theta = \frac{F\sin^4\theta + G\cos^4\theta + H\cos^2 2\theta + 0.5N\sin^2 2\theta}{F\sin^2\theta + G\cos^2\theta} - 1. \tag{7}$$

The identification of the anisotropy parameters for the Hill'48 yield criterion is based in the experimental yield stresses and the experimental coefficients of plastic anisotropy presented in Table 2. Since the identification of the hardening law was obtained with the stress–strain curve along the RD, the uniaxial yield stress at 0° with the RD was selected. Therefore, the condition $G + H = 1$ is imposed, leading to $\sigma_0 = 172$ MPa, which is the initial yield stress given by the hardening law, being slightly different from the experimental value (see Table 2). In the classical approach (Hill'48-R), the yield function is defined using three experimental coefficients of anisotropy $r_0$, $r_{45}$ and $r_{90}$ and the uniaxial yield stress $\sigma_0$. On the other hand, the identification of the yield criterion with the approach labelled by 'Hill'48-S' is performed by using the three experimental values of the yield stress $\sigma_0$, $\sigma_{45}$ and $\sigma_{90}$ and the experimental coefficient of anisotropy $r_0$. The same condition ($G + H = 1$) is applied in the second approach due to the same reasons. Table 3 presents the material parameters of the Hill'48 yield criterion, identified using Eqs. (6) and (7), for both approaches considered.

The identification of the anisotropy parameters for the Yld'91 yield criterion takes into account both the experimental yield stresses and the coefficients of plastic anisotropy, which are listed in Table 2. The procedure used is based on the minimization of an error function that evaluates the difference between the predicted and the experimental values. The objective error function is defined as:

**Table 3**
Identified material parameters for the Hill'48 and Yld'91 yield criteria.

| Hill 1948 | | | | | | |
|---|---|---|---|---|---|---|
| Label | $F$ | $G$ | $H$ | $L$ | $M$ | $N$ |
| Hill'48-R | 0.3137 | 0.3663 | 0.6337 | 1.5000 | 1.5000 | 1.1764 |
| Hill'48-S | 0.3224 | 0.3663 | 0.6337 | 1.5000 | 1.5000 | 1.4658 |

| Barlat 1991 | | | | | | | |
|---|---|---|---|---|---|---|---|
| Label | $c_1$ | $c_2$ | $c_3$ | $c_4$ | $c_5$ | $c_6$ | $m$ |
| Yld'91 | 0.8396 | 0.8846 | 1.0979 | 1.0000 | 1.0000 | 0.9111 | 6 |

$$\text{error} = w_\sigma \sum \left(\frac{\sigma_\theta}{\sigma_\theta^{\exp}} - 1\right)^2 + w_r \sum \left(\frac{r_\theta}{r_\theta^{\exp}} - 1\right)^2, \tag{8}$$

where the $\sigma_\theta$ and $\sigma_\theta^{\exp}$ are the predicted and experimental uniaxial yield stresses along the direction $\theta$ with the rolling direction, respectively. The variables $r_\theta$ and $r_\theta^{\exp}$ denote the predicted and experimental anisotropy coefficients along the direction $\theta$ with the rolling direction, respectively. This error function considers different weight values for the experimental yield stress and the anisotropy coefficient. However, in this study it was considered that all experimental values were equally weighted. Besides, since the material crystallography of the mild steel is BCC, the value of exponent $m$ was fixed to 6. As in the case of Hill'48 yield criterion, the parameters defining the anisotropy through the thickness are assumed isotropic, which means that $c_4 = c_5 = 1.0$. Table 3 presents the material parameters of the Yld'91 yield criterion identified using the objective function described in Eq. (8).

The uniaxial anisotropy coefficient distribution in the plane of the sheet, predicted using different yield criteria is presented in Fig. 5. Both the Hill'48-R and the Yld'91 model fit accurately the experimental values, while the Hill'48-S model leads to an $r$-value distribution closer to the normal anisotropy behaviour. The initial uniaxial yield stress distribution in the sheet's plane, predicted by the various yield criteria studied is shown in Fig. 6. Since the Hill'48-S model was obtained based on the yield stresses, the predicted distribution fits exactly the experimental distribution, but shifted down 4 MPa due to the difference introduced by the Swift law. The yield stress distribution predicted by the Yld'91 model is situated between the Hill'48-R and the Hill'48-S models. The yield surfaces predicted by different yield criteria are shown in Fig. 7 for the $\sigma_{xx} - \sigma_{yy}$ plane. Both models that adopt the Hill'48 yield criterion present similar surfaces, being the predicted surface clearly outside the von Mises yield locus along the biaxial stress axis since $r > 1$ (cf. Fig. 5). The biaxial yield stress predicted by the Yld'91 model is between the value obtained with the Hill'48 and the von Mises yield criterion. Fig. 3 presents the stress–strain curves obtained from the uniaxial tensile tests performed numerically at 0°, 45° and 90° with the RD for each yield criterion studied. Comparing with the experimental curves, the predicted evolution is adequate at the RD for all yield criteria analysed (see Fig. 3(a)). However, at 45° with the RD, the numerical curves are rather distant from the experimental one, as shown in Fig. 3(b), particularly for the Hill'48-R model, where the predicted curve lies about 50 MPa above the experimental one. The predicted stress–strain curves at 90° with the RD adopting the anisotropic yield criteria are slightly above the experimental one, as shown in Fig. 3(c).

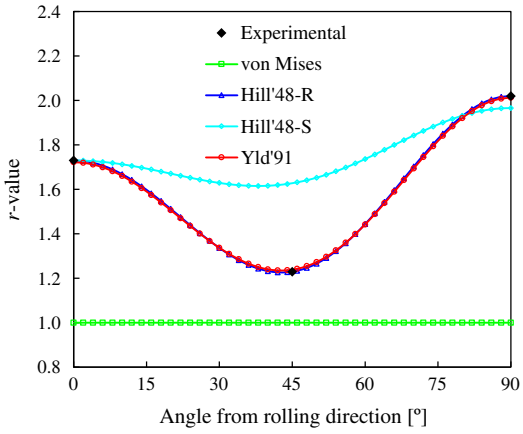


**Fig. 5.** Comparison between experimental and predicted anisotropy coefficient distribution for different yield criteria.

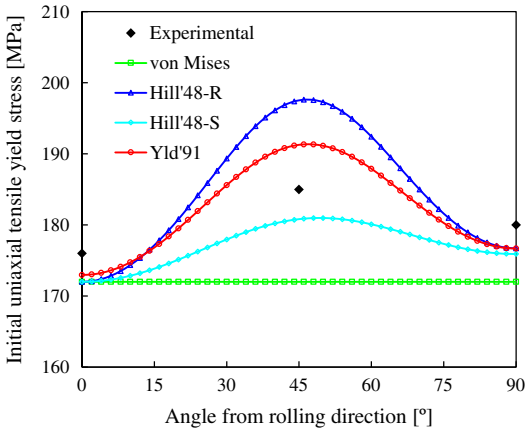


**Fig. 6.** Comparison between experimental and predicted initial uniaxial yield stress distribution for different yield criteria.

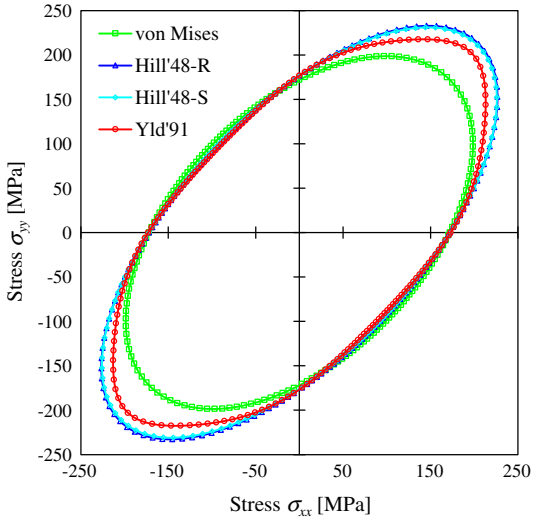


**Fig. 7.** Yield surfaces predicted by different yield criteria.

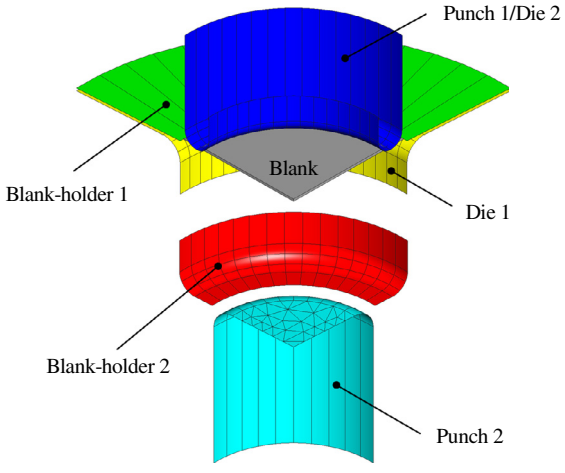


**Fig. 8.** Discretization of the forming tool surfaces with Nagata patches.

### 3.3. Simulation conditions

Due to geometric and material symmetry conditions, only one quarter of the model is simulated, as shown in Fig. 8. The main dimensions of the forming tools used in the reverse deep drawing process are presented in Table 4. The tools are considered as rigid and its surfaces are discretized with Nagata patches, presented in Fig. 8 [27], being the required normal vectors for the smoothing method evaluated using the algorithm proposed by Neto et al. [32]. The circular blank has 170 mm diameter and 0.98 mm of initial thickness. One-fourth of the blank is discretized with 8-node hexahedron solid finite elements, combined with a selective reduced integration technique [33]. The total number of elements is 15,408, using 2 layers of elements through the thickness. The friction coefficient between sheet and tools is taken from the benchmark specifications as $\mu = 0.15$. The cylindrical cup is fully drawn in both process stages of the reverse deep drawing, which correspond to about 60 mm of punch displacement in the first stage and 90 mm in the second stage. Since the cylindrical cup is a closed geometry, the amount of springback between forming stages is very small, being not analysed in this study. A detailed study about the springback in cylindrical cups can be found in Zein et al. [34]. Although, typically the blank-holder is controlled by force, the effect of fixed blank-holder gap in deep drawing of square cups was studied by Gavas and Izciler [35], concluding that the best forming quality is attained when the gap ranges from 1.0 to 1.3 times the initial sheet thickness. In the present example, the gap between the die and the blank-holder is held fixed in both stages. Its value was determined experimentally in order to draw a cylindrical cup without wrinkles, being set equal to 1.13 mm in the first stage and 1.4 mm in the second stage [19].

**Table 4**
Forming tool dimensions in mm.

| Tool geometry | Stage 1 | Stage 2 |
|---|---|---|
| Die opening diameter | 104.5 | 78.0 |
| Die radius | 8.0 | 5.5 |
| Die height | 21.0 | 16.0 |
| Punch diameter | 100.0 | 73.4 |
| Punch radius | 5.5 | 8.5 |
| Blank-holder opening diameter | 104.5 | 75.0 |
| Blank-holder radius | – | 7.0 |
| Blank-holder height | – | 20.0 |

## 4. Results and discussion

This section is devoted to the comparison between numerical and experimental results, performed for both stages of the forming process. All experimental results presented in this study are available from the conference proceedings, being selected the ones carried out by Kim et al., from Kangwon National University, for DDQ mild steel [14]. In fact, only two participants delivered all results for the fully reverse deep drawing process, being the blank-holder gap used in the presented experimental results equal to the one specified in the study of Thuillier et al. [19].

### 4.1. Punch force evolution

The comparison between experimental and numerical punch force evolution during the first forming stage is shown in Fig. 9. The experimental evolution is well predicted by all yield criteria studied, although globally the numerical force evolution is slightly lower than the experimental one. Nevertheless, the oscillations observed in the numerical results of Thuillier et al. [15], related to contact between the deformed mesh and the tools, are completely eliminated in the present work due to correct selection of blank discretization and accurate tool surface description [36]. The sudden increase of the punch force, approximately at 37 mm of displacement, for the model that assumes isotropic material behaviour (von Mises), results from the ironing of the flange (see

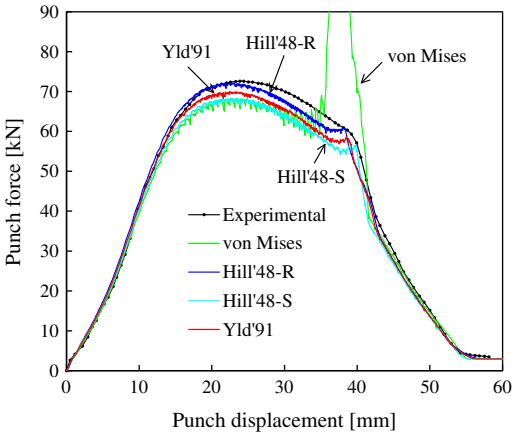


**Fig. 9.** Comparison between experimental and predicted punch force evolution during the 1st stage, using different yield criteria.

Fig. 9). Since the deformation mode of the flange is situated between pure shear and uniaxial compression (region of thickening), the isotropic behaviour ($r = 1$) leads to a sheet thickening higher than the one obtained with an anisotropy characterized by an $r > 1$, as observed through Eq. (5). Once the gap between the die and the blank-holder is held fixed, the increasing thickness in the flange leads to an increase of the blank-holder contact force, which is directly replicated in the punch force due to high restraining forces.

Concerning the second stage, Fig. 10 presents the comparison between experimental and numerical punch force evolutions. Globally, the experimental evolution is accurately predicted by the numerical model, whatever the yield criterion adopted. In fact, the force evolution is better predicted in the present study than in the work of Thuillier et al. [15], which takes into account kinematic hardening. However, all models predict a decrease of the punch force for a punch displacement lower than the experimental one, although the slope is correctly predicted. The punch force evolution obtained with the Yld'91 model, which seem to be closer to the experimental one, is located between the results achieved with the Hill'48 yield criterion, using the two approaches for material parameters identification. Indeed, the Hill'48-S model and the von Mises yield criterion lead to similar results in terms of punch force evolution. In both stages of the reverse deep drawing process, the punch force predicted by the Hill'48-R model is always higher than using the Hill'48-S model, which is related with the uniaxial yield stress at 45° with the RD (see Fig. 6). The same tendency can be observed in the stress–strain curves of Fig. 3(b), performed numerically for both models, which highlight the higher strength of the material described with the Hill'48-R model than with Hill'48-S model.

### 4.2. Earing profile

The earing profile is defined by the height of the deep drawing cup measured along the circumferential direction of the cup using the angle with the RD. The predicted earing profiles after the forward and reverse fully deep drawing operations are compared in Fig. 11. These earing profiles were not compared with experimental ones, since they are not available. The influence of the selected yield criteria on the earing profile is evident, being always predicted four ears when anisotropic yield functions are used (the same number of ears observed in the experiments [19]). Since the level of plastic deformation increases during the reverse redrawing (higher drawing ratio), the amplitude of the ears is enlarged from the first to the second drawing stage. Moreover, the amplitude predicted with the Hill'48-R model is considerable higher than the one obtained using the Hill'48-S model, because in the last case the $r$-value distribution in the plane of the sheet presents a lower variation, as observed in Fig. 5. Although the $r$-value distribution dictated by Hill'48-R and Yld'91 is very similar (see Fig. 5), the amplitude of the ears at 45° with the RD is considerably inferior for the Yld'91 model. This is motived by the inferior variation of the uniaxial yield stress distribution for the Yld'91 model (Fig. 6), since the yield stress profile description is as important as the $r$-value one, as pointed by Yoon et al. [37].

### 4.3. Strain distribution/evolution

The equivalent plastic strain distribution predicted by the Yld'91 yield criterion at the end of first stage is presented in Fig. 12. The maximum value reached is approximately 0.6, being located somewhat under of the ears placed at 0° and 90° with the RD. In fact, the value of equivalent plastic strain in the cup wall, for the same cup height, is lower at 45° than at 0° and 90° with the RD, which is in accordance with the earing profile (see Fig. 11). Fig. 13 shows the equivalent plastic strain distribution predicted by the Yld'91 yield criterion at the end of second stage. The maximum value attained is approximately 1.1, being situated in the same localization defined in the first stage. Note that all studied anisotropic yield criterion give similar equivalent plastic strain distributions. Since the hardening law was identified using the

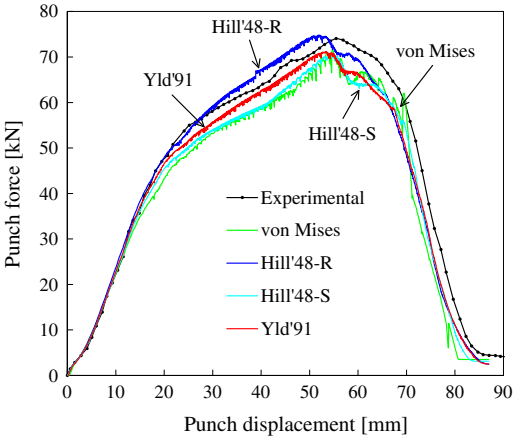


**Fig. 10.** Comparison between experimental and predicted punch force evolution during the 2nd stage, using different yield criteria.

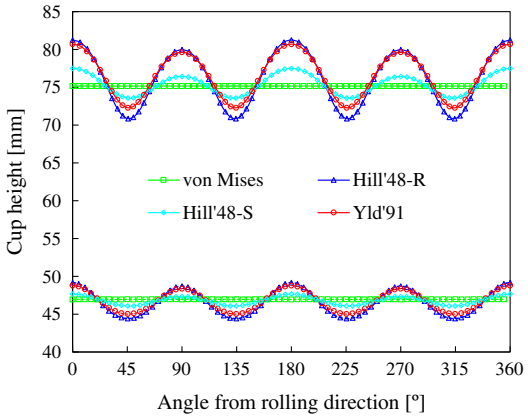


**Fig. 11.** Comparison of the earing profiles after 1st (dashed line) and 2nd (solid line) drawings, obtained with different yield criteria.

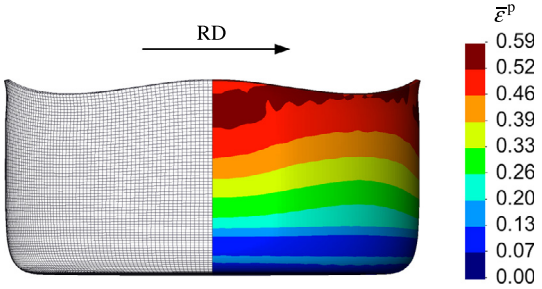


**Fig. 12.** Equivalent plastic strain distribution at the end of 1st stage, predicted by the Yld'91 yield criterion.

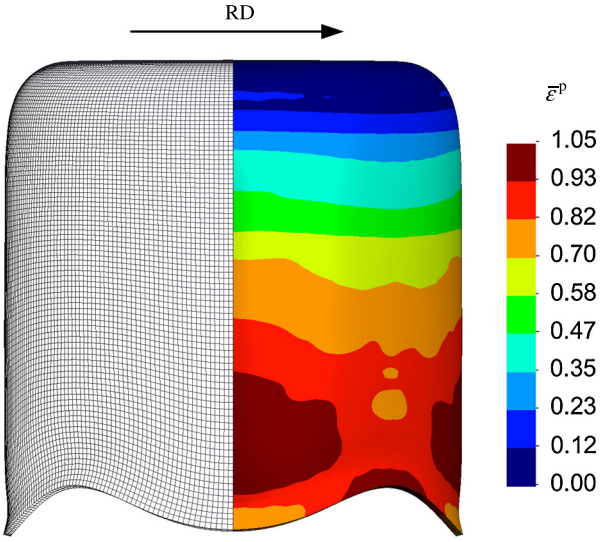


**Fig. 13.** Equivalent plastic strain distribution at the end of 2nd stage, predicted by the Yld'91 yield criterion.

uniaxial tensile tests, where the strain range is about 22% before necking (see Fig. 3), the hardening behaviour for higher strain values is extrapolated by the Swift law. In fact, the high strain values obtained in the deep drawing process, which can be observed in the equivalent plastic strain distribution, result from the occurrence of multi strain paths (not only uniaxial tension).

Thuillier et al. [15] analysed the occurrence of strain path changes in this two-stage deep drawing process, considering the interior peel of the sheet to highlight the Bauschinger effect. In this study, the analysis is focused on the strain paths predicted by the different yield criteria. Hence, the influence of the plastic anisotropy on the strain distribution/evolution is analysed comparing the anisotropic models with the results obtained in isotropy (von Mises), highlighting the differences observed at different directions with the RD. Fig. 14 presents the evolution of minor–major strain distribution during the first stage of drawing, predicted by both the von Mises and the Yld'91 yield criteria in the exterior peel of the sheet. The magnitude of the major strain at 45° with the RD is closer to the one predicted assuming isotropy, particularly at the end of forming stage. Moreover, during the forming process, both the minor and major predicted strains are always higher at 0° and 90° than at 45° with the RD, which is in agreement with the equivalent plastic strain plotted in Fig. 12. In fact, the higher *r*-values predicted by the Yld'91 anisotropic model at 0° and 90° with the RD (see Fig. 5), when compared with the von Mises criterion, dictates higher values of deformation in the sheet's plane, which is the cause to the arise of the four ears in the cup. The high restraining forces in the blank-holder (flange ironing) predicted by

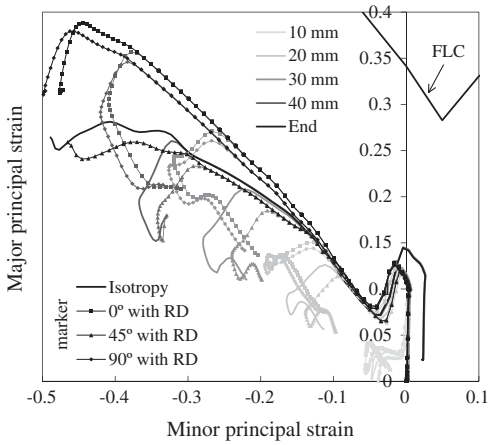


**Fig. 14.** Comparison of minor–major strain distribution during the 1st stage for isotropy and anisotropy described by Yld'91 yield criterion (measured in exterior peel of the cup).

the isotropic yield criterion during the drawing (Fig. 9) leads to the stretching of the sheet near the punch radius. This is consequence of the equal biaxial strain path imposed in that zone between 30 and 40 mm of punch displacement, as can be observed in Fig. 14.

In order to identify the deformation modes occurring during the first forming stage, in each sector of the cylindrical cup, nine material points of the exterior peel were selected. They are located from 45 mm to 85 mm of the initial radial distance, regularly spaced every 5 mm. Fig. 15 presents the evolution of minor–major strain predicted by von Mises yield criterion for the selected points. The isotropic yield criterion is selected in order to analyse only one section of the cylindrical cup, leading to an axisymmetric problem. Moreover, the anisotropic behaviour changes the strain paths, making the analysis more complex due to its deviation from the conventional strain paths (uniaxial compression, pure shear, plane strain) [15]. Since the blank-holder force is small due to the fixed gap imposed, the strain path in the flange of the deep draw cup is approximately uniaxial compression ($\varepsilon_2 = -2\varepsilon_1$), region where the sheet thickens due to the circumferential compression. Thus, the higher values of major strains predicted by the Yld'91 yield criteria at 0° and 90° with the RD (see Fig. 14) are dictated by the uniaxial compression, which is characterized in anisotropy by a strain path $\varepsilon_2 = -a\varepsilon_1$, being $a < 2$ when $r > 1$. On the other hand, the points

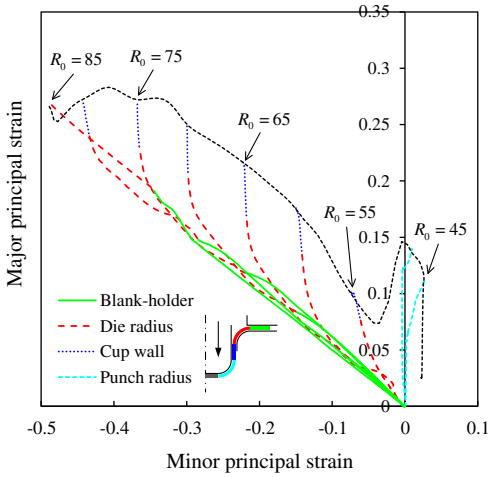


**Fig. 15.** Evolution of minor–major strain (deformation modes) predicted for nine material points of the exterior peel during 1st stage, assuming isotropy.

located in the cup wall are submitted to plane strain ($\varepsilon_2 = 0$) since the sheet extends only in the axial direction, being the circumferential straining prevented by the punch. The variation of the strain path arises in the die radius, ranging from uniaxial compression to plane strain, as shown in Fig. 15. The points situated in the punch radius are subjected to plane strain followed by biaxial stretching. Nevertheless, the biaxial stretching only occur for the von Mises yield criterion (see Fig. 14) because of the flange ironing.

The comparison of minor–major strain distribution during the second stage, predicted by both the von Mises and the Yld'91 yield criteria in the outside peel of the sheet, is shown in Fig. 16. Although the strain distribution predicted by the Yld'91 yield criterion at 45° with the RD is closer to the one predicted assuming isotropy, the difference between them at the end of forming is higher than the one obtained in the first stage. The magnitude of the major strain at the end of the cup's wall for a direction with 45° to the RD is significantly inferior to the one predicted at 0° and 90°, which is related with the ears development. Indeed, the height of the ear at 0° is higher than at 90° with the RD (see Fig. 11) since the predicted major strain is larger at 0° with the RD during all forming process.

The strain path evolution is also analysed during the reverse deep drawing stage, using six material points of exterior peel defining the cup, which are positioned from 35 mm to 85 mm of the initial radial distance, regularly spaced every 10 mm. Fig. 17 presents the evolution of minor–major strain for the selected points, considering isotropic material behaviour (von Mises). The strain paths predicted for the reverse redrawing are similar to the ones found in the first stage. When the sheet flows between the die and blank-holder, the strain path evolution is approximately uniaxial compression (blank-holder gap 1.4 mm). On the other hand, the sliding of the sheet on the die radius leads to a strain path that starts between uniaxial compression and pure shear ($\varepsilon_2 = -\varepsilon_1$) and change quickly to plane strain near the transition to the cup's wall, where the path evolution is approximately plane strain, as shown in Fig. 17. The points situated in the punch radius are subjected to pure shear followed by plane strain. Note that the main strain path occurring in the reverse redrawing is close to uniaxial compression, which happens both for material points in contact with the blank-holder and with the die radius. The strain paths observed during the drawing process (see Figs. 15 and 17) allow establish relations to evaluate analytically the earing profile after reverse deep drawing using [37].

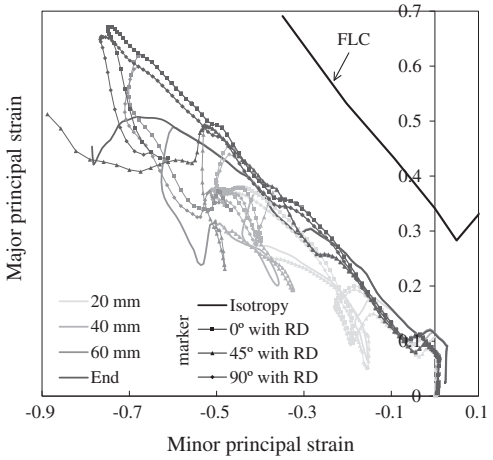


**Fig. 16.** Comparison of minor–major strain distribution during the 2nd stage for isotropy and anisotropy described by Yld'91 yield criterion (measured in exterior peel of the cup).

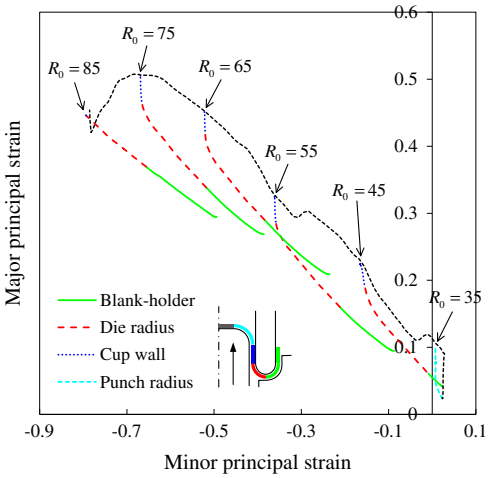


**Fig. 17.** Evolution of minor–major strain (deformation modes) predicted for six material points of the exterior peel during 2nd stage, assuming isotropy.

### 4.4. Thickness distribution

Both the experimental and the numerical thickness distributions presented in this section were calculated in the radial direction, always perpendicular to the cylindrical cup axis. Note that the predicted thickness distribution is directly correlated with the strain distribution analysed in the previous section, as well as the strain paths existent in the deep drawing process [23]. Fig. 18(a) presents the comparison between experimental and predicted cup wall thickness distribution at the end of the first stage, in the RD direction. The predicted thickness distribution using both anisotropic yield criteria (Hill'48 and Yld'91) lead to similar results, which are very close to the experimental one, particularly when the Hill'48-S model is adopted. On the other hand, applying the von Mises yield criterion, the thickness is clearly overestimated for a cup height superior to 10 mm and underestimated for the lower cup height. Fig. 18(b) presents the experimental and predicted cup wall thickness distribution at 45° with the RD. The predicted thickness distribution using any of the presented yield criteria lead to similar results for the cup height superior to 10 mm, which overestimate slightly the experimental distribution. For the cup height inferior to 10 mm, only the Yld'91 yield criterion predicts accurately the experimental thickness distribution. The comparison between experimental and predicted cup wall thickness distribution at 90° with the RD is shown in Fig. 18(c). The experimental thickness is overestimated by the numerical models, being the Yld'91 yield criterion the more accurate in opposition to the von Mises, which gives the worst results.

The sheet thinning predicted by the von Mises yield criterion in the transition between punch radius and cup wall (cup height equal to 5.5 mm), for all studied directions, is associated with the flange ironing (abrupt increase of the punch force shown in Fig. 9) and the lower biaxial yield stress, as indicated in Fig. 7. Moreover, the thickness is overestimated by the same yield criterion for all three directions analysed due to the lower value of the anisotropy coefficient ($r = 1$), which is particularly evident at 0° and 90° with the RD, as shown in Fig. 18(a and c), respectively. On the other hand, the thickness predicted by both anisotropic yield criteria (Hill'48 and Yld'91) leads to satisfactory results in all directions, presenting a maximum difference to the experimental values inferior to 3.5%. Indeed, the thickness distribution predicted by the Yld'91 yield criterion, when taking into account all directions analysed, is in general the more accurate model, being the difference to the experimental values always inferior to 1.5%. Since at the end of forming stage, the strain distribution predicted

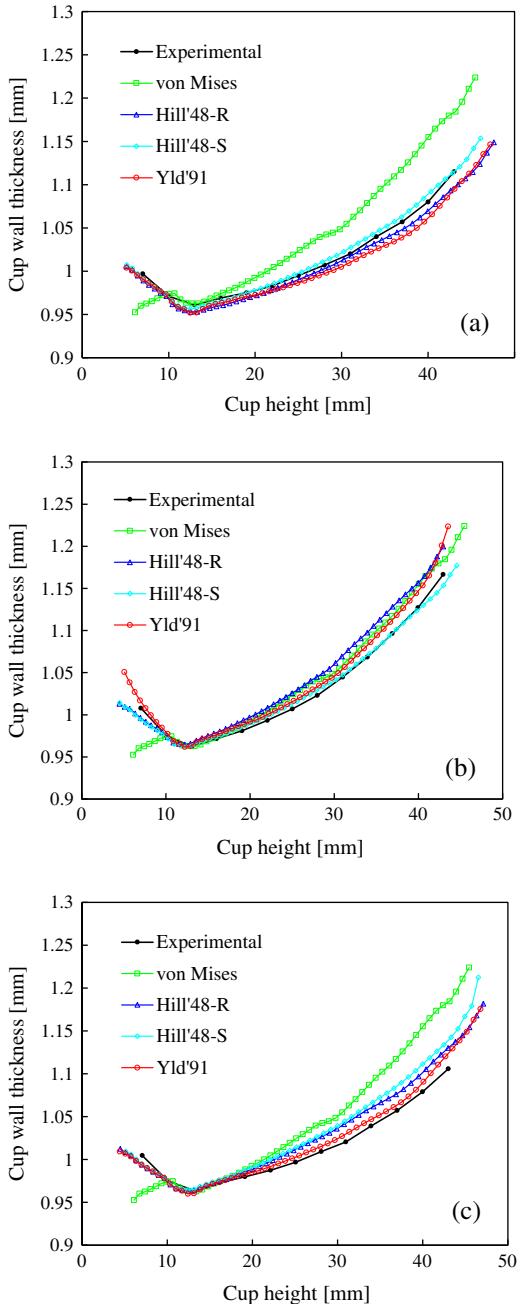


**Fig. 18.** Experimental and numerical thickness distribution in the cup wall after 1st stage at: (a) 0° with the RD; (b) 45° with the RD; and (c) 90° with the RD.

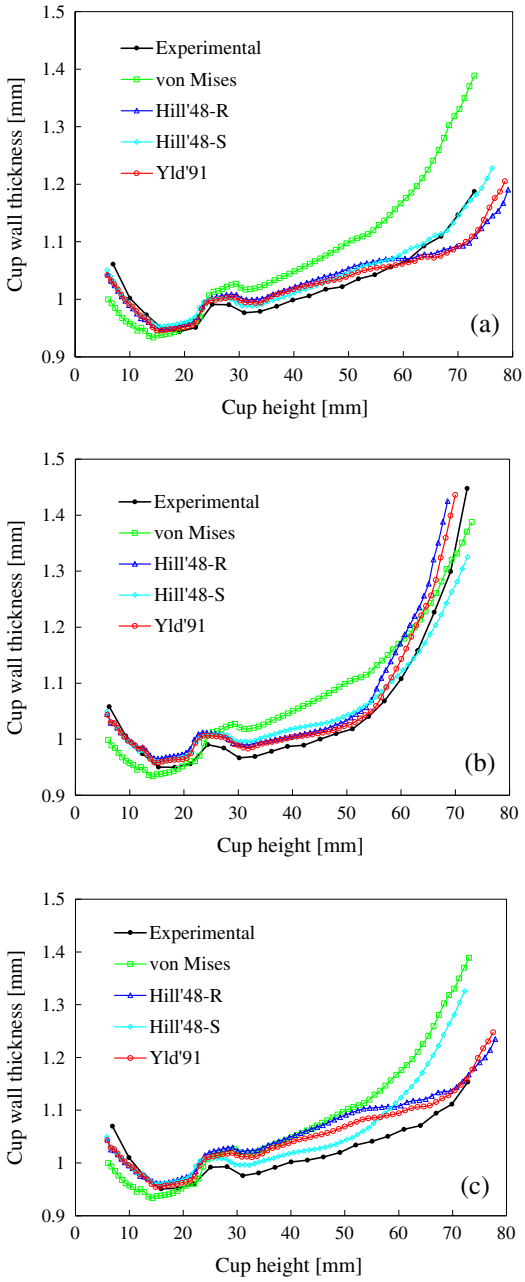


**Fig. 19.** Experimental and numerical thickness distribution in the cup wall after 2nd stage at: (a) 0° with the RD; (b) 45° with the RD; and (c) 90° with the RD.

by the Yld'91 yield criterion at 45° with the RD is close to the one predicted assuming isotropy (Fig. 14), the thickness distribution at this direction is similar for both yield criteria, as shown in Fig. 18(b). Besides, the predicted thicknesses at 0° and 90° are inferior to the one at 45° with the RD (same trend observed experimentally) because higher values of major strain were predicted at 0° and 90° with the RD, as shown in Fig. 14.

The thickness predicted by the numerical model at the end of the second stage is directly influenced by the thickness distribution obtained in the first stage, becoming its numerical evaluation more challenging due to the error accumulation attained after each forming stage [19]. The comparison between experimental and predicted cup wall thickness distribution at the end of the second stage in the RD direction is shown in Fig. 19(a). The thickness distributions obtained with the Hill'48-R and Yld'91 yield criteria are analogous, while the prediction obtained with Hill'48-S model provides the numerical result closer to the experimental one, particularly for a cup height superior to 60 mm. Fig. 19(b) compares the experimental and predicted cup wall thickness distribution at 45° with the RD. The results obtained with the Hill'48-R and Yld'91 yield criteria are similar, being the ones closer to the experimental distribution, which is slightly overestimated. Indeed, the final slope in the thickness distribution is accurately predicted using these models, in contrast with the von Mises and Hill'48-S models. Fig. 19(c) contains the comparison between experimental and predicted thickness distribution along the cup wall at 90° with the RD. The thickness is overestimated by all studied yield criteria, with both the Hill'48-R and Yld'91 models predicting a thickness distribution closer to the experimental tendency. Nevertheless, the thickness is better predicted by the Hill'48-S model until a

cup height of 55 mm, being excessively overestimated by this model for higher values of the cup's height.

The sheet thickness is underestimated by the Von Mises yield criterion in the three directions at the end of second stage, for a cup height inferior to 20 mm, since the excessive thinning predicted in the first stage dictates irreversibly the result of the following forming stages. Note that the equal biaxial strain occurring in the first stage, due to flange ironing (Fig. 14), is reproduced in the strain distribution of the second stage, as can be observed in Fig. 16. In fact, the material points located at a cup's height inferior to 10 mm in the first stage correspond to a cup's height inferior to 30 mm at the end of second stage. On the other hand, for a cup height superior to 25 mm the thickness is overestimated in all directions, following the same trend observed in at the end of the first stage, as can be seen comparing Figs. 18 and 19. Although the Hill'48-S provides accurate results for the thickness distribution along the RD, the predicted thickness at 45° and 90° with the RD are not so well predicted, being clearly overestimated at 90° with the RD for a cup height superior to 55 mm. The wall thickness for a cup height superior to 55 mm, predicted by both anisotropic yield criteria, is substantially higher at 45° than at 0° and 90° with the RD, as presented Fig. 19. This difference results from the lower value of major strain at the end of the cup's wall (approximately last 20 mm) for a direction 45° with the RD, as shown in Fig. 16. Globally, the Yld'91 yield criterion is the more accurate model when taking into account all directions analysed (difference to experimental inferior to 4%), particularly at 45° with the RD, following the same trend observed in the first stage. Nevertheless, the gap between experimental and numerical thickness is higher at the end of second stage than in the first stage, whatever the yield criterion adopted.

Fig. 20 presents the thickness strain distribution in the cylindrical cup at the end of the first stage, predicted by both the Hill'48-S yield criterion (left side) and the Yld'91 yield criterion (right side). The results are in accordance with the cup wall thickness distribution shown in Fig. 18. For both models, the negative thickness strain in the transition between punch radius and cup wall is more evident in the RD than in transverse direction. The Yld'91 yield criterion predicts more pronounced ears (see Fig. 11), being the thickness strain at 45° with the RD globally higher than at the RD and the transverse direction. The thickness strain distribution in the cup at the end of the second stage is shown in Fig. 21. The differences between yield criteria are higher in the second stage, being the maximum thickness strain values located at 45° with the RD in the end of cup wall. Since the Yld'91 yield criterion allows a higher range for the *r*-values (see Fig. 5), the predicted thickness strain is more heterogeneous along the circumferential direction. The plateau in the cup wall thickness at 45° with the RD (see Fig. 19(b), between 25 and 55 mm of cup height) is highlighted in Fig. 21.

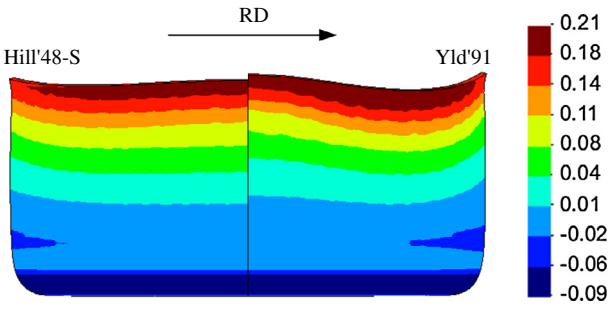


**Fig. 20.** Predicted thickness strain distribution at the end of 1st stage, using both the Hill'48-S yield criterion (left side) and Yld'91 yield criterion (right side).

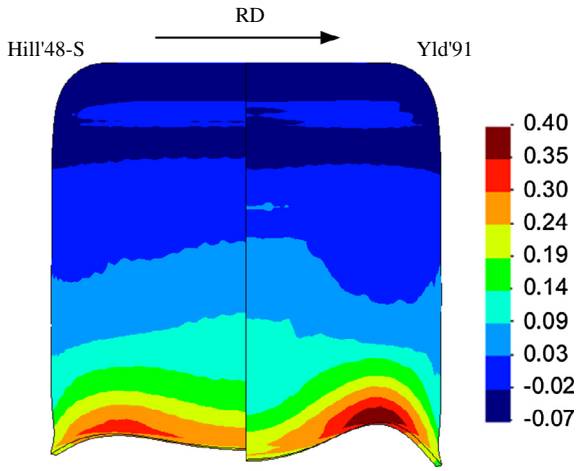


**Fig. 21.** Predicted thickness strain distribution at the end of 2nd stage, using both the Hill'48-S yield criterion (left side) and Yld'91 yield criterion (right side).

## 5. Conclusions

This study deals with the three dimensional numerical simulation of the reverse deep drawing process of a cylindrical cup, being the numerical results compared with the experimental ones. The anisotropic behaviour of the mild steel sheet is described by both the Hill'48 yield criterion and the more advanced non-quadratic yield criteria Yld'91, in addition to the isotropic von Mises yield criterion. Moreover, the anisotropy coefficients for the Hill'48 function were identified based either on the yield stresses or the *r*-values measured in three different material orientations from the uniaxial tensile tests.

The numerical analysis allows identifying the strain paths associated to each cup region during each forming stage, which are similar in both stages. The material flow between the die and the blank-holder is subjected to uniaxial compression, changing to plane strain in the cup wall. The important strain path changes occur in the die radius, ranging from uniaxial compression to plane strain. Moreover, the comparison of minor-major strain distribution at different orientations with the RD allows establishing a direct relationship with the obtained wall thickness distribution. The differences observed in the strain distribution for different angles with the RD are consequence of the *r*-values and yield stresses predicted by each yield criterion and the strain paths generated during the forming process.

The cup wall thickness distribution is strongly influenced by the yield criteria, particularly when comparing isotropic and anisotropic behaviour. Indeed, at the end of first stage, the thickness predicted by the von Mises model at 0° and 90° with the RD is clearly higher than the one predicted by both the Hill'48 and Yld'91 yield criteria. Besides, the differences in the predicted thickness distribution between anisotropic yield criteria are small in all the analysed directions, being the numerical distribution close to the experimental one. Concerning the cup wall thickness at the end of the second stage, its numerical prediction is somewhat worse than in the first stage, being the thickness globally overestimated in all directions. Nevertheless, both the Hill'48-R and Yld'91 models predict a thickness distribution close to the experimental tendency, in particular the Yld'91 yield criterion. In conclusion, since the Yld'91 non-quadratic yield function is identified using both the uniaxial yield stress and uniaxial anisotropy coefficient at three different material orientations, the numerical thickness distribution is closer to the experimental results in both forming stages. The punch force evolution is accurately predicted in both forming stages whatever the anisotropic yield criteria adopted, since it is only slightly affected by the yield criterion.

## Acknowledgements

The authors gratefully acknowledge the financial support of the Portuguese Foundation for Science and Technology (FCT) via the projects PTDC/EMS-TEC/1805/2012 and PEst-C/EME/UI0285/2013 and by FEDER funds through the program COMPETE – Programa Operacional Factores de Competitividade, under the project CENTRO-07-0224-FEDER-002001 (MT4MOBI). The first author is also grateful to the FCT for the PhD Grant SFRH/BD/69140/2010.

## References

[1] Tekkaya AE. State-of-the-art of simulation of sheet metal forming. J Mater Process Technol 2000;103:14–22.
[2] Makinouchi A. Sheet metal forming simulation in industry. J Mater Process Technol 1996;60:19–26.
[3] Dixit US, Joshi SN, Davim JP. Incorporation of material behavior in modeling of metal forming and machining processes: a review. Mater Des 2011;32:3655–70.
[4] El Sherbiny M, Zein H, Abd-Rabou M, El Shazly M. Thinning and residual stresses of sheet metal in the deep drawing process. Mater Des 2014;55:869–79.
[5] Gantar G, Pepelnjak T, Kuzman K. Optimization of sheet metal forming processes by the use of numerical simulations. J Mater Process Technol 2002;130–131:54–9.
[6] Menezes LF, Teodosiu C. Three-dimensional numerical simulation of the deep-drawing process using solid finite elements. J Mater Process Technol 2000;97:100–6.
[7] Yoon JW, Barlat F, Dick RE, Chung K, Kang TJ. Plane stress yield function for aluminum alloy sheets–Part II: FE formulation and its implementation. Int J Plast 2004;20:495–522.
[8] Hill R. A theory of the yielding and plastic flow of anisotropic metals. Proc R Soc Lon 1948;193:281–97.
[9] von Mises R. Mechanik der festen Körper im plastisch-deformablen Zustand, Nachrichten von der Gesellschaft der Wissenschaften zu Göttingen. Mathematisch-Physikalische Klasse 1913:582–92.
[10] Hosford WF. Limitations non-quadratic anisotropic yield criteria and their use in analyses of sheet forming. ASM Int 1988:163–70.
[11] Kim S, Lee J, Barlat F, Lee M-G. Formability prediction of advanced high strength steels using constitutive models characterized by uniaxial and biaxial experiments. J Mater Process Technol 2013;213:1929–42.
[12] Barlat F, Lege DJ, Brem JC. A six-component yield function for anisotropic materials. Int J Plast 1991;7:693–712.
[13] Cazacu O, Barlat F. Generalization of Drucker's yield criterion to orthotropy. Math Mech Solids 2001;6:613–30.
[14] Gelin JC, Picart P. Benchmark C: reverse deep drawing of a cylindrical cup. In: Gelin JC, Picart P, editors. Proceedings of Numisheet'99. France: Besançon; 1999. p. 871–932.
[15] Thuillier S, Manach PY, Menezes LF. Occurrence of strain path changes in a two-stage deep drawing process. J Mater Process Technol 2010;210:226–32.
[16] Min DK, Jeon BH, Kim HJ, Kim N. A study on process improvements of multi-stage deep-drawing by the finite-element method. J Mater Process Technol 1995;54:230–8.
[17] Cao J, Li S, Xia ZC, Tang SC. Analysis of an axisymmetric deep-drawn part forming using reduced forming steps. J Mater Process Technol 2001;117:193–200.
[18] Marciniak Z, Duncan JL, Hu SJ. Mechanics of Sheet Metal Forming. second ed. New York: Butterworth-Heinemann; 2002.
[19] Thuillier S, Manach PY, Menezes LF, Oliveira MC. Experimental and numerical study of reverse re-drawing of anisotropic sheet metals. J Mater Process Technol 2002;125–126:764–71.
[20] Chung SY. Stress analysis of reverse redrawing of cylindrical shells. Sheet Met Ind 1951;28:453–8.
[21] Zharkov VA. Theory of the drawing of cylindrical parts from sheet materials. J Mater Process Technol 1992;31:379–92.
[22] Teodosiu C, Daniel D, Cao H-L, Duval J-L. Modelling and simulation of the can-making process using solid finite elements. J Mater Process Technol 1995;50:133–43.
[23] Kim SH, Kim SH, Huh H. Finite element inverse analysis for the design of intermediate dies in multi-stage deep-drawing processes with large aspect ratio. J Mater Process Technol 2001;113:779–85.
[24] Kim HK, Hong SK. FEM-based optimum design of multi-stage deep drawing process of molybdenum sheet. J Mater Process Technol 2007;184:354–62.
[25] Parsa MH, Yamaguchi K, Takakura N. Redrawing analysis of aluminum–stainless-steel laminated sheet using FEM simulations and experiments. Int J Mech Sci 2001;43:2331–47.
[26] Alart P, Curnier A. A mixed formulation for frictional contact problems prone to Newton like solution methods. Comput Methods Appl Mech Eng 1991;92:353–75.
[27] Neto DM, Oliveira MC, Menezes LF, Alves JL. Applying Nagata patches to smooth discretized surfaces used in 3D frictional contact problems. Comput Method Appl Mech Eng 2014;271:296–320.
[28] Menezes LF, Neto DM, Oliveira MC, Alves JL. Improving computational performance through HPC techniques: case study using DD3IMP in-house code. AIP Conf Proc 2011;1353:1220–5.
[29] Tresca HE. Mémoire sur l'écoulement des corps solides soumis à de fortes pressions. Comp Rend Acad Sci (Paris) 1864;59:754.
[30] Hosford WF. A generalised isotropic yield criterion. J Appl Mech 1972;39:607–9.
[31] Logan RW, Hosford WF. Upper-bound anisotropic yield locus calculations assuming ⟨111⟩-pencil glide. Int J Mech Sci 1980;22:419–30.
[32] Neto DM, Oliveira MC, Menezes LF, Alves JL. Nagata patch interpolation using surface normal vectors evaluated from the IGES file. Finite Elem Anal Des 2013;72:35–46.
[33] Hughes TJR. Generalization of selective reduced integration procedures to anisotropic and nonlinear media. Int J Num Meth Eng 1980;15:1413–8.
[34] Zein H, El Sherbiny M, Abd-Rabou M, El Shazly M. Thinning and spring back prediction of sheet metal in the deep drawing process. Mater Des 2014;53:797–808.
[35] Gavas M, Izciler M. Effect of blank holder gap on deep drawing of square cups. Mater Des 2007;28:1641–6.
[36] Neto DM, Oliveira MC, Menezes LF, Alves JL, Manach PY. Applying Nagata patches in the description of smooth tool surfaces used in sheet metal forming simulations. Key Eng Mater 2013;554–557:2277–84.
[37] Yoon JW, Dick RE, Barlat F. A new analytical theory for earing generated from anisotropic plasticity. Int J Plast 2011;27:1165–84.